JCTC Journal of Chemical Theory and Computation

On the Competition between Predissociation and Direct Dissociation in Deuterium Chloride Ions (DCl^+)

Mikhail V. Korolkov[†,‡] and Karl-Michael Weitzel*[‡]

Stephanov Institute of Physics, National Academy of Science, Nezavisimosti ave. 70, 220602 Mink, Republic of Belarus, and Philipps Universität Marburg, Fachbereich Chemie, Hans Meerwein Strasse, 35032 Marburg, Germany

Received July 4, 2006

Abstract: The competition between direct dissociation and predissociation in DCl^+ ions prepared in the $A^2\Sigma^+$ state has been investigated numerically by solving the time dependent Schrödinger equation. This work concentrates on the rovibronic states (v_A;N_A) with $v_A = 8$ and $N_A = 60-65$, which are close to the top of a centrifugal barrier. We find that the relative yield of D^+ (by direct dissociation) and Cl^+ (by predissociation) strongly depends on the excitation frequency, intensity, and duration. Investigation of the time dependence of the product yields provides evidence for significant multichannel interactions.

I. Introduction

The competition between different possible reaction channels lies at the heart of chemical research, with the ultimate goal to find selectivity for the formation of one specific product, e.g. in asymmetric catalysis[1−3] or to control the outcome of this competition.[4−6] One important piece of the mosaic is the understanding of competition at the molecular level, in particular the dynamical aspect. In the attempt to control chemical dynamics currently two types of approach are being pursued in the literature: the frequency domain approach[7] and the time domain approach.[8]

In the current work we investigate the competition of direct dissociation with predissociation in deuterium chloride ions (DCl^+). The formation of HCl^+ and DCl^+ ions has been investigated extensively by resonance enhanced multiphoton ionization (REMPI)[9−12] but also single photon ionization in the VUV.[13−16] The internal state distribution of ions has been analyzed both by means of classical photoelectron spectroscopy[17,18] but also by photodissociation spectroscopy.[19] The spectroscopy of the ion is also well-known.[19−21] The energetically lowest dissociation limit in the DCl^+ ion corresponds to the formation of Cl^+ and D. The second dissociation limit corresponds to the formation of D^+ and Cl. The energetics of these two dissociation channels and the thresholds relevant for their competition are illustrated in Figure 1.

Here, the lowest fragmentation threshold T_1 (formation of Cl^+) is given by the energetic limit of the ion ground state ($X\ ^2\Pi_{3/2}$) and three repulsive potential curves ($^4\Sigma^-$, $^2\Sigma^-$, $^4\Pi$). The dissociation limit of the first excited electronic state of DCl^+ ($A\ ^2\Sigma^+$) converges to the formation of D^+ (threshold T_3). In the general situation of nonzero rotational angular momentum both bound potentials will exhibit a centrifugal barrier, denoted as T_2 in the ion ground state and T_4 in the A state. Note, that both T_2 and T_4 depend on the corresponding rotational quantum number N. Between the energies T_1 and T_3 formation of Cl^+ is possible by direct dissociation of the ion ground state or by predissociation of the A state. The latter becomes possible by spin−orbit coupling to the three nominally repulsive electronic states, $^4\Sigma^-$, $^2\Sigma^-$, and $^4\Pi$. Above T_3 formation formation of D^+ is accessible by direct dissociation from the A state, which will consequently compete with predissociation. Between T_3 and T_4 this direct dissociation requires tunneling, which is slow compared to predissociation. It is only in the region very close to the top of the barrier T_4 that the direct dissociation of the A state can effectively compete with the predissociation. This competition is the subject of the current work.

II. Computational Techniques

In the current work the dissociation dynamics of DCl^+ ions have been investigated by numerical solution of time

* Corresponding author e-mail: weitzel@chemie.uni-marburg.de.
† National Academy of Science.
‡ Philipps Universität Marburg.

10.1021/ct600217t CCC: $33.50
Published on Web 10/04/2006

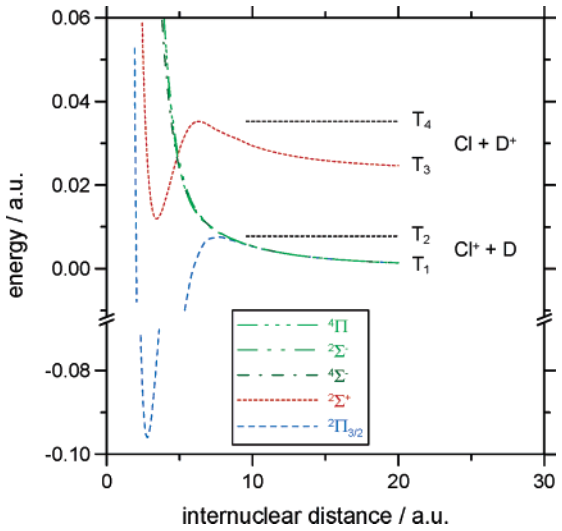

Figure 1. Schematic plot of the potential energy curves relevant for the fragmentation of DCl^+ together with 4 different thresholds. For further discussion see the text (1 au = a_o = 0.5292 Å).

dependent, coupled Schrödinger equations. Similar approaches have been described in previous papers.[22−24] A full account will be given below.

The input used for the wave packet calculations is based on ab initio data from Dalgarno et al.,[25] which were slightly adjusted in order to reproduce known spectroscopic parameters.[14,19,26] The current work takes into account those five different electronic states discussed above: (i) the ion ground state (X $^2\Pi_{3/2}$, j=1), (ii) the first excited electronic state (A $^2\Sigma^+$, j=2), and (iii) three repulsive states, $^4\Sigma^-$ (j=3), $^2\Sigma^-$ (j=4), and $^4\Pi$ (j=5). For these states coupled Schrödinger equations have been set up as given below[27]

$$i\hbar\frac{\partial\Psi_X(r,t)}{\partial t} = [\hat{T} + \tilde{V}_X]\Psi_X(r,t) + \eta_{X,A}(r)E_z(t)\Psi_A(r,t) + \eta_{X,4}(r)E_z(t)\Psi_4(r,t) \quad (1)$$

$$i\hbar\frac{\partial\Psi_A(r,t)}{\partial t} = [\hat{T} + \tilde{V}_A]\Psi_A(r,t) + \eta_{A,X}(r)E_z(t)\Psi_X(r,t) + \sum_{j=3}^{5} H^{so}_{A,j}(r)\Psi_j(r,t) \quad (2)$$

$$i\hbar\frac{\partial\Psi_3(r,t)}{\partial t} = [\hat{T} + \tilde{V}_3]\Psi_3(r,t) + H^{so}_{A,3}(r)\Psi_A(r,t) \quad (3)$$

$$i\hbar\frac{\partial\Psi_4(r,t)}{\partial t} = [\hat{T} + \tilde{V}_4]\Psi_4(r,t) + \eta_{4,X}(r)E_z(t)\Psi_X(r,t) + H^{so}_{4,A}(r)\,\Psi_A(r,t) \quad (4)$$

$$i\hbar\frac{\partial\Psi_5(r,t)}{\partial t} = [\hat{T} + \tilde{V}_5]\Psi_5(r,t) + H^{so}_{5,A}(r)\Psi_A(r,t) \quad (5)$$

where the potential energy in the relevant electronic states is given by

$$\tilde{V}_x = V_x + \frac{J_X\cdot(J_X+1) - \Omega_X{}^2}{2\cdot\mu\cdot r^2} \quad (6)$$

$$V_A = V_A + \frac{N_A\cdot(N_A+1)}{2\cdot\mu\cdot r^2} + 0.5\cdot\gamma\cdot N_A \quad (7)$$

$$\tilde{V}_j = V_j + \frac{J_j\cdot(J_j+1) - \Omega_j{}^2}{2\cdot\mu\cdot r^2} \quad (8)$$

for j = 3 ($^4\Sigma^-$), 4 ($^2\Sigma^-$), and 5 ($^4\Pi$).

V_X, V_A, and V_j are the ab initio potential energies of the X-, A-, and the three repulsive states, respectively, to which the appropriate rotational energy is added. Here we use two different types of transitions: (i) $J_X = N_A + 0.5$ (Q_1 transition) and (ii) $J_X = N_A - 0.5$ (R_1 transition), further $J_j = N_A + 0.5$, and $\gamma(DCl^+) = 0.25$ cm^{-1}. Note, that for the ground electronic X state and the repulsive $^4\Sigma^-$, $^2\Sigma^-$, and $^4\Pi$ states, Hund's case (a) representation was chosen, for the A state Hund's case (b) applies. The data shown in Figure 1 are for DCl^+ with N_A = 62. For the bound, ground state Ω_X = 1.5, for the three repulsive states Ω_j = 1.5. The reduced mass is $\mu(D^{35}Cl^+)$ = 3542.23 au (au = atomic units). In general the five states (and thus the Schrödinger equations) are coupled via spin−orbit interaction, $H^{so}_{A,j}(r)$, and through optical excitation, e.g. $\eta_{X,A}(r)E_z(t)$, where $\eta_{X,A}(r)$ is the transition dipole moment connecting states X and A. The radial dependence of the latter is taken into account. Note, that the model is based on DCl^+ ions oriented along the x axis. The spin−orbit coupling matrix elements were taken from ref 23. The optical excitation will be discussed below.

In previous work we have shown that the predissociation lifetime can be reasonably approximated by a free decay model in which optical excitation is neglected. In the current work we are explicitly interested in the optical excitation spectrum inducing the dissociation.[26,19,28,20] Therefore we are looking at the decay of a wave function in a laser field. For this approach optical excitation starting from the ion ground state is taken into account by means of a realistic laser pulse. Spin−orbit coupling is taken into account from the beginning.

The laser field was represented by the following function

$$E(t) = \begin{cases} E_o\cdot\sin^2\left[\frac{\pi\cdot t}{t_1}\right]\cdot\sin(\omega t) & \text{for } 0 \le t \le t_l \\ 0 & \text{for } t > t_l \end{cases} \quad (9)$$

where t_l is characterizing the width of the laser pulse at the base. Typically t_l = 80 ps was chosen in this work. This corresponds to a FWHM of the intensity profile of 29 ps.

Direct optical coupling is only taken into account between states A and X and $^2\Sigma^-$ and X, respectively. Spin−orbit coupling is only taken into account between the A state and the three repulsive states but not between the A state and the X state. The latter would only be relevant, if we considered emission processes, which is not the case, and also only at significantly longer times.

The five nuclear wave functions are represented on an equidistant M-point spatial grid with $r = (r_1, r_2, ..., r_M)$, $r_1 = 1.5a_o$, $r_{i+1} - r_i = 0.02a_o$, for 4096 < M < 32 768, which allows to use fast Fourier transform (FFT) methods for the transformation between coordinate and momentum space.[29] A combination of the split-operator method[30] and the integral

equation method[31,32] is used for the propagation of the wave functions (given in eqs 1−5) in time with time steps of $\Delta t \leq 1$ atomic unit (1 au ≈ 0.024 fs). The total propagation time (identical to the laser pulse duration) is chosen as appropriate for the corresponding fragmentation dynamics. Typically this total time is about 1 order of magnitude larger than the respective lifetime. This ensures that the line width derived does not depend on the laser pulse duration. The absorbing boundary[33] is used to prevent the artificial reflection of all $\Psi_j(r, t)$ wave functions at the edge of the grid, where necessary.

All calculations deal with the dynamics of the vibronic $A^2\Sigma^+$ (v_A=8) state, with rotational angular momentum ranging from $N_A = 60$ to $N_A = 65$.

III. Results

III.1. Results for Target States (v_A=8;N_A) in Weak Laser Fields. We start this result section with the discussion of the (v_A;N_A) = (8;60) state under conditions of excitation by a very weak laser field. This state is relatively short-lived.[27] The $N_A = 60$ state is located roughly 2400 cm^{-1} above the limit for direct dissociation (T_3) but 450 cm^{-1} below the top of the centrifugal barrier (T_4).

In Figure 2 we show the normalized absorption spectrum (yield spectrum), $Y_{abs} = (1 - \langle\Psi_X|\ \Psi_X\rangle)$, calculated at the end of propagation with the target state $N_A = 60$. The spectrum also shows the relative contribution of the three predissociation channels k_j. This relative contribution is defined as

$$k_j = \frac{\mathrm{Flux}(\Psi_j(r_o,t))}{\sum_{j=3}^{5}\mathrm{Flux}(\Psi_j(r_o,t))}$$

where the flux is calculated at an internuclear separation of $r_o = 20$ au

$$\mathrm{Flux}(\Psi_j(r_o,t)) = \frac{\hbar}{2\cdot i\cdot m}\cdot\left[\Psi^*_j(r_o,t)\cdot\left(\frac{\partial\Psi_j(r,t)}{\partial r}\right)_{r\to r_o} - \Psi_j(r_o,t)\cdot\left(\frac{\partial\Psi^*_j(r,t)}{\partial r}\right)_{r\to r_o}\right]$$

Despite the fact that the (8;60) state is lying above T_3, only predissociation occurs. This implies that direct dissociation is much slower than predissociation. This in turn is due to tunneling being required for the direct process. Among the three predissociation channels state $^4\Pi$ (j=5) clearly dominates. This is connected to the crossing point between the bound A state and the repulsive states, where at the relevant internuclear distance of about 4.5 au the spin−orbit coupling matrix element is largest for this channel j = 5. Evidently the fraction k_5 is basically independent of the excitation frequency, k_4 slightly increases, and k_3 slightly decreases with excitation frequency.

By fitting a Lorentzian function to the numerical data we derive a lifetime of 409 fs. For comparison we performed calculations for the free decay of eigen states. In the latter case the optical excitation step is not included in the numerical calculations.[23,27] For this free decay a lifetime of 411 fs is obtained in very good agreement with the optically induced decay. We note, however, that the numerical data in Figure 2 show a small deviation from Lorentzian line shape. On the low-frequency wing of the spectrum, the numerical data are above; on the high-frequency wing of the spectrum the numerical data are below the best Lorentzian line fit. An experiment aimed at detecting this deviation from Lorentzian line shape would require a high signal/noise ratio on the order of 50. The absorption spectrum with the target state $N_A = 61$ is shown in Figure 3. This rotational state, $N_A = 61$, is still about 330 cm^{-1} below the top of the barrier (T_4 for $N_A = 61$). For this and all higher states predissociation and direct dissociation can effectively compete. This competition is the topic of the current manuscript. Here, for $N_A = 61$ the contribution from direct dissociation is only 0.3%, despite the fact that the state $N_A = 61$ is relatively long-

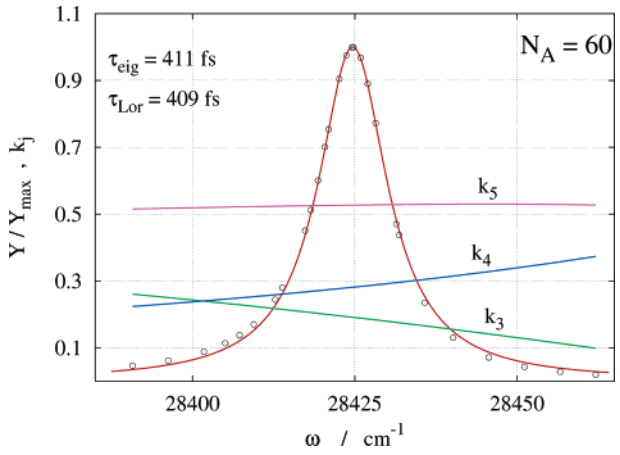

Figure 2. Normalized absorption spectrum of the DCl^+ into the $v_A = 8$, $N_A = 60$ state (Q_1 transition): symbols: numerical data; line: Lorentzian function. Relative contribution of the three repulsive states to the overall predissociation process as a function of the excitation frequency (labeled k_3, k_4, and k_5).

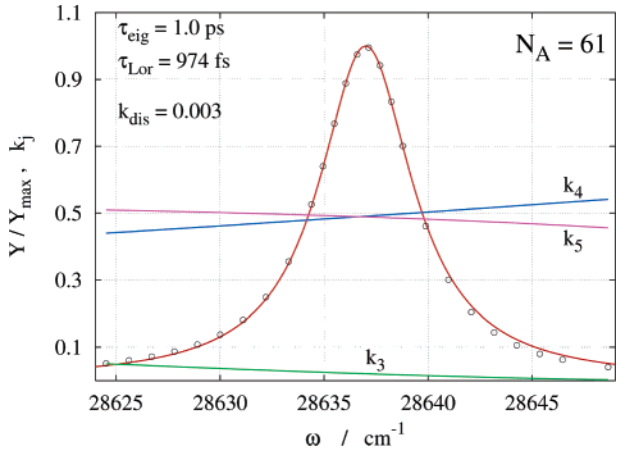

Figure 3. Normalized absorption spectrum of the DCl^+ into the $v_A = 8$, $N_A = 61$ state (R_1 transition): symbols: numerical data; line: Lorentzian function. Relative contribution of the three repulsive states to the overall predissociation process as a function of the excitation frequency (labeled k_3, k_4, and k_5).

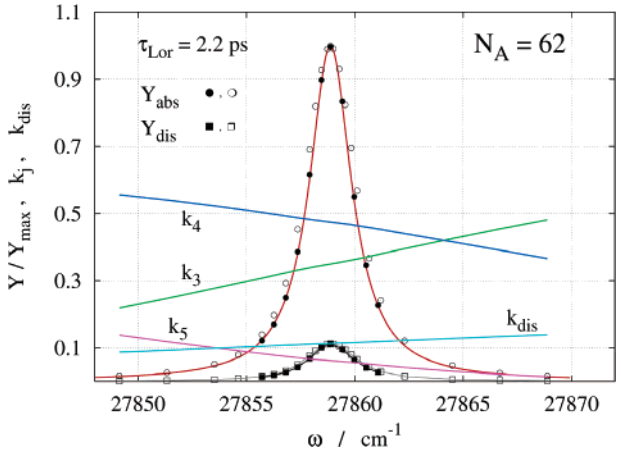

Figure 4. Normalized absorption spectrum of the DCl^+ into the $v_A = 8$, $N_A = 62$ state (Q_1 transition): symbols: numerical data (● ■: 80 ps, ○ □: 40 ps); red line: Lorentzian function fitted to ●. The line through the ■ and □ data is the result of spline. Relative contribution of the three repulsive states to the overall predissociation process as a function of the excitation frequency (labeled k_3, k_4, and k_5).

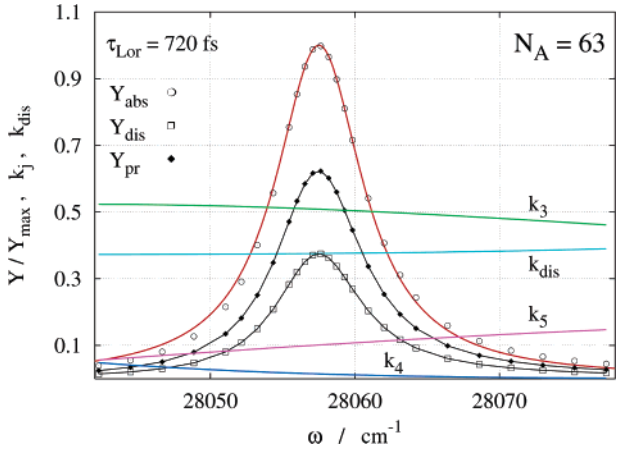

Figure 5. Normalized absorption spectrum of the DCl^+ into the $v_A = 8$, $N_A = 63$ state (R_1 transition): symbols: numerical data; red line: Lorentzian function fitted to ○. Lines through Y_{dis} and Y_{pr} data are result of spline. Relative contribution of the three repulsive states to the overall predissociation process as a function of the excitation frequency (labeled k_3, k_4, and k_5).

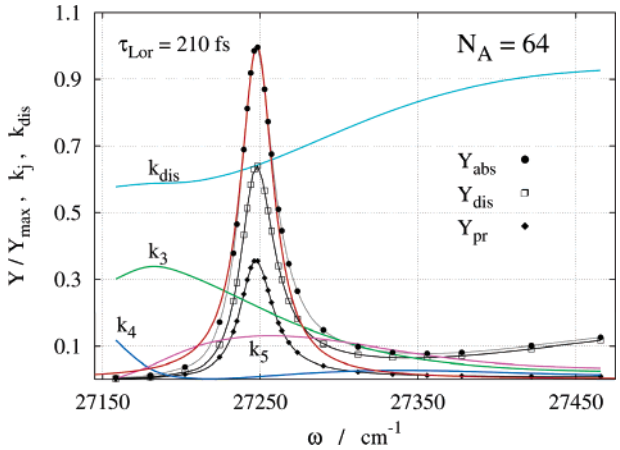

Figure 6. Normalized absorption spectrum of the DCl^+ into the $v_A = 8$, $N_A = 64$ state (Q_1 transition): symbols: numerical data; red line: Lorentzian function fitted to Y_{abs}. Black and gray lines through data points are the result of spline. Relative contribution of the three repulsive states to the overall predissociation process as a function of the excitation frequency (labeled k_3, k_4, and k_5).

lived. A Lorentzian fit to the numerical data leads to τ = 974 fs. The free decay of eigenstates leads to $\tau = 1$ ps, again in good agreement. While channel 5 clearly dominated for $N_A = 60$, here predissociation is dominated by channel j = 4 and $j = 5$, and channel $j = 3$ contributes less than 5%. The frequency dependence of all k_j is weak. However, there is again a noticeable asymmetry in the frequency dependence of Y_{abs}, similar to the situation for $N_A = 60$. Figure 4 shows the absorption spectrum leading to the target state $N_A = 62$. This state still lies 216 cm^{-1} below T_4 ($N_A = 62$). During the course of the investigation it turned out, that this is the longest living state considered in this work. Thus it was deemed appropriate to check for possible contributions of the laser pulse duration on the calculated lifetime. Therefore numerical calculations have been performed for two different total laser pulse durations (propagation times), i.e., 40 and 80 ps (τ(FWHM) $\approx$ 14.6 and 29 ps). Evidently, the absorption profile (Y_{abs}) is slightly more narrow for 80 ps compared to 40 ps. Since the difference is small, we conclude that 80 ps are long enough to accurately represent the dynamics. Consequently a lifetime of $\tau = 2.2$ ps has been derived from a Lorentz fit to the numerical absorption spectrum. The contribution of direct dissociation to the total flux is about 10%. A free decay of eigenstates has no meaning in this case and is therefore not available for comparison. In terms of channel competition the total flux in $N_A = 62$ is dominated by channels $j = 3$ and $j = 4$. Channel $j = 5$ contributes even less than the direct dissociation for the major part of the spectrum. The spectral characteristics of Y_{abs} and Y_{diss} are very similar. This implies that also predissociation and dissociation have very similar spectral characteristics. Figure 5 shows the absorption spectrum leading to the target state $N_A = 63$. For this state, which lies 113 cm^{-1} below T_4 ($N_A = 63$), the lifetime is 720 fs. The contribution of k_{diss} to the entire flux is about 38%, independent of the frequency. Fifty percent of the total flux goes into the predissociation through channel $j = 3$. Channel $j = 5$ contributes about 10%, and k_4 is negligible again with weak frequency dependence. In a later section we will discuss the influence of the laser pulse intensity and duration on the product yield for this target state. Figure 6 shows the absorption spectrum leading to the target state N_A = 64. In 0th order this state lies 29 cm^{-1} below T_4 (N_A=64). This vicinity to T_4 leads to significant deviation from Lorentzian line shape for all yield data ($Y_{abs} = Y_{dis} + Y_{pr}$). To get at least a rough figure of the order of magnitude of τ, we have included a Lorentzian line fitted to the FWHM of the data Y_{abs} (red line). This leads to $\tau = 210$ fs. Evidently k_{dis} increases from 0.6 on the low-frequency wing of the spectrum to above 0.9 at 150 cm^{-1} above the center frequency. This increase in k_{dis} is most likely connected to the vicinity to the top of the centrifugal barrier to direct

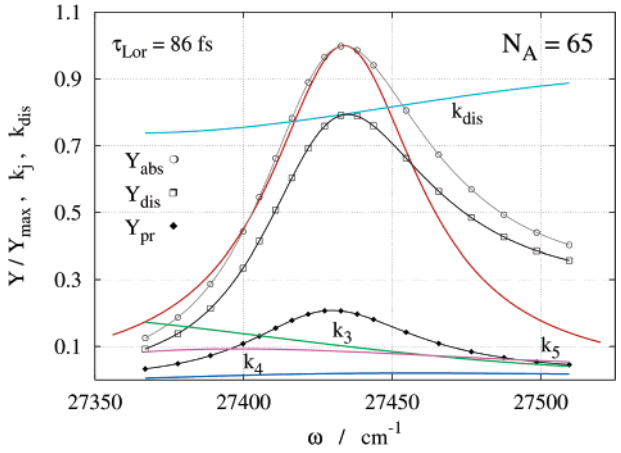

Figure 7. Normalized absorption spectrum of the DCl^+ into the $v_A = 8$, $N_A = 65$ state (R_1 transition): symbols: numerical data; red line: Lorentzian function fitted to Y_{abs}. Black lines through data points: spline. Relative contribution of the three repulsive states to the overall predissociation process as a function of the excitation frequency (labeled k_3, k_4, and k_5).

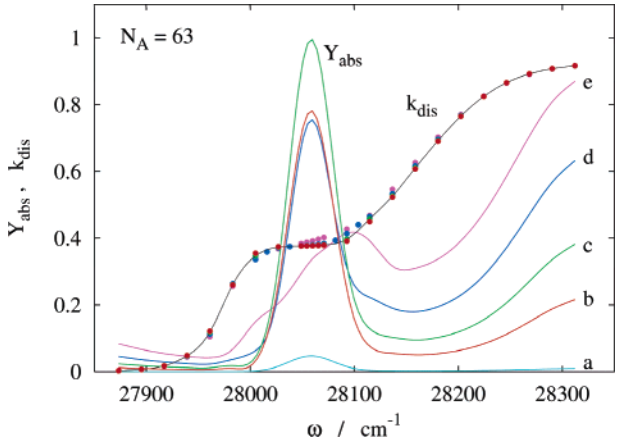

Figure 8. Absolute absorption yield spectrum of the DCl^+ into the $v_A = 8$, $N_A = 63$ state for various laser fields: a: 0.0001 au, b: 0.005 au, c: 0.007 au, d: 0.01 au, e: 0.014 au.

dissociation. It is automatically (due to normalization) reflected in a decrease of k_3 and also k_4. However, on the high-frequency wing of the spectrum k_4 slightly increases again. Channel $j = 5$ shows a resonancelike variation with ω. The increase in k_{dis} is associated with the deviation from Lorentzian line shape on the high frequency wing of the spectrum. Most likely the reason for both is that the lifetime for direct dissociation changes much faster than that for predissociation in this region. This effect appears to be smooth, indicating that there are no sharp steps in the corresponding lifetimes. Figure 7 shows the absorption spectrum leading to the target state $N_A = 65$. This is the first state which lies above the top of the centrifugal barrier (4 cm^{-1}). Therefore direct dissociation leading to the formation of D^+ dominates. Yet, k_{dis} still increases from 0.75 to 0.9 over a range of 100 cm^{-1}. States $j = 3$ and $j = 5$ each contribute on the order of 10% at the center frequency, slightly decreasing with ω, the contribution of channel $j = 4$ is almost negligible.

The numerical data for Y_{abs} are very non-Lorentzian on the high ω wing of the spectrum. Obviously, in this situation the derivation of a lifetime is problematic. To get an estimate of the magnitude of τ we have fitted a Lorentzian to the low ω wing of the data. From this analysis we obtain a lifetime $\tau = 86$ fs. This is considered to be a very short lifetime. In previous work[27] we showed that the lifetime between the rotational islands of stability increased with the RIS index from about 90 fs to 200 fs. The lifetime of the (8;65) state is even shorter than the shortest lifetimes calculated between the threshold and the first RIS (cf. Figure 2 of ref 27). The asymmetry discussed above for Y_{abs} is even more pronounced in Y_{dis} but less pronounced for Y_{pr}. This is indicative of significant multichannel interactions. In classical kinetics one would expect the same line shape for directly competing processes. We will come back to this point below.

III.2. Results for Different Laser Pulse Intensities and Duration. All the calculations described above utilized very low laser fields of maximum amplitude $E = 0.000025$ au (1 au $= E_{hartree}/(e \cdot a_o) = 5142$ MV/cm), such that the calculated absolute absorbance was only on the order of a few %, i.e., in the linear regime. At the same time the laser pulse width were always chosen significantly larger than the total dissociation lifetime. This ensured that any spectral result was unaffected by laser pulse properties. In the following we discuss results for various laser field strength and also for shorter laser pulse width. Most of these calculations were performed for the $N_A = 63$ state. Figure 8 shows the absolute absorbance yield spectrum for various laser fields between 0.005 au to 0.014 au. The laser pulse width is in each case 1 ps. As it turns out, the absorbance, in particular the absorbance at the center transition frequency, is a strongly varying function of the laser field strength. For low fields the absorbance increases with the power, as expected for the linear regime. At high laser fields the absorbance in general exhibits a maximum followed by oscillatory behavior. The precise laser field for which the absorbance becomes maximum depends on the target state and also the excitation frequency and the pulse duration. For the current condition the highest peak absorbance is observed for an intermediate laser field of 0.007 au (trace c in Figure 8). The corresponding intensity is $I_o = 0.5 \cdot \epsilon_o \cdot c \cdot E_o^2 = 3.5 \cdot 10^{16}$ W/cm$^2 \cdot E_o^2$, where E is given in atomic units. For this field, which is a factor 280 higher than that in Figure 5, the maximum absorbance is $Y_{abs} = 1$. For laser fields above and below this special value the maximum absorbance at the center frequency is smaller. Even more interesting is the spectral characteristics of the absorbance and the ratio of direct dissociation to predissociation on the high-frequency wing of the excitation spectrum. Here, the contribution of direct dissociation to the total flux, k_{dis}, increases between 28 100 and 28 300 cm^{-1} from about 0.4 to 0.9. It is important to emphasize that the increase in Y_{abs} does not represent a transition to the next higher rotational state, since only a single final rotational state is included in these calculations. Rather, the increase in k_{dis} is mostly likely related to surpassing the top of the barrier for direct dissociation. While the fractional yield of direct dissociation at a given excitation frequency does not depend on the laser field, the absolute absorbance does increase with increasing laser field strength amplitude in the region of the top of this barrier (around 28 300 cm^{-1}). Since

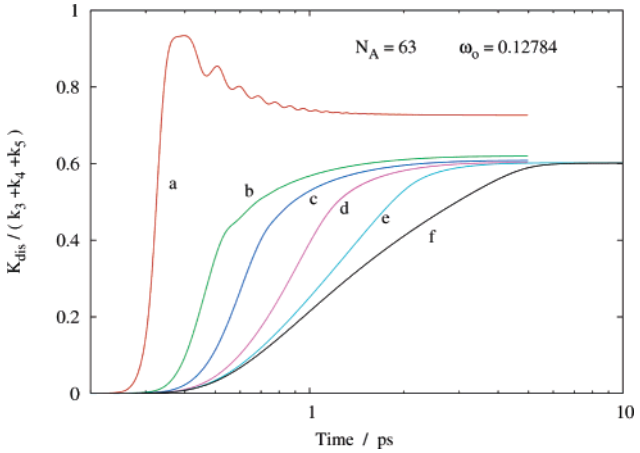

Figure 9. Time dependence of the branching ratio $k_{dis}/k_{prediss}$ for various laser pulse duration: a: 0.1 ps, b: 0.3 ps, c: 0.5 ps, d: 1 ps, e: 2 ps, f: 5 ps.

the square of the laser field amplitude scales with the laser intensity (see above), this implies an increasing absolute yield of absorbance with increasing intensity. It is interesting to note that a similar result for the spectral absorbance is obtained in calculations, where the laser pulse duration is varied, but the laser field amplitude is kept constant.

Another interesting aspect is the time dependence of the individual channel contributions. In classical kinetics the branching ratio of directly competing chemical processes is time independent. We may now ask the question: down to what time regime is this picture valid. At zero time all molecules are in their ground state. With propagation in time the flux through the available channels increases. For laser pulse duration larger than 0.3 ps the yield of direct dissociation increases smoothly with time, approaching a limiting value of $k_{dis} = 0.38$. However, for pulse duration of 0.1 ps k_3 first increases steeply to about 0.48 and decreases then with time, approaching a limiting value 0.42. This is a first indication of multichannel dynamics. The time dependence of the predissociation yield exhibits nonmonotonic behavior with transient maxima for all laser pulses between 0.1 and 5 ps. Again, this result would not be expected in classical kinetics. Finally in Figure 9 we present the time dependence of the branching ratio between direct dissociation and predissociation for laser pulses with durations between 0.1 and 5 ps. For all these laser pulse durations considered the branching ratio reaches a time independent value after several picoseconds. However, this limiting value is not approached in a step function but either by a monotonic increase for long pulses or by a nonmonotonic increase for pulse duration of 0.1 ps. We note that the limiting value for 0.1 ps differs from that for longer laser pulses. The time dependence of the branching ratio $k_{dis}/(k_3+k_4+k_5)$ directly reflects the time dependence of the interaction between the different electronic states involved. While this is in fact not surprising from the dynamical point of view, the interesting aspect is that the fingerprint of this interaction ceases after several picoseconds and the response of the system changes from pure dynamical to classical kinetic behavior.

IV. Summary

We have investigated the competition between direct dissociation (formation of D^+) and predissociation (formation of Cl^+) for high lying rovibrational states $v_A = 8$, $N_A = 60-65$ in the region of the top of a centrifugal barrier in the $A^2\Sigma^+$ state of DCl^+. Direct dissociation becomes important starting from about 100 cm^{-1} below the top of this barrier via tunneling. Analysis of the omega dependence of the channel yields reveals significant multichannel interactions. The individual channel yields vary strongly with omega but also with time. In classical kinetics directly competing chemical reaction channels lead to a time independent product ratio. In the fragmentation of DCl^+ multichannel interaction leads to a pronounced time dependence of product branching ratios. This can be rationalized as being due to a time dependence of the effective cross section for population transfer between individual levels. In principle this time dependence could in part originate from the time dependence of the laser field. We note, however, that multichannel interactions are also predicted in calculations which do not take into account the laser field.[22] More likely the multichannel dynamics reflect the microreversibility of population flow between the different electronic states involved. In the long time limit—reached after several picoseconds—a transition to classical kinetics is observed. For the future it would be interesting to perform similar calculations also for $v_A = 9$ and 10, since for these vibrational levels the corresponding N_A quantum numbers would be significantly lower and therefore more easy to access experimentally.

The photochemical processes considered in the current work have been induced by one photon absorption from the ion X state into the electronic excited A state. An alternative access to the competition between dissociation and predissociation is provided by femtosecond multiphoton excitation in the IR or mid-IR. As an example we mention the competition between direct dissociation of NaI, leading to the formation of $Na^\bullet$ and $I^\bullet$, and predissociation, leading to Na^+ and I^-, as investigated theoretically by Engel and coworker.[34] For the title molecule of the current work we have reported evidence for the possibility to control the competing product channels D^+ vs Cl^+ in a fs experiment employing 800 nm pulses.[35]

Acknowledgment. Support of this work from the DFG (436 WER 17/4/02 and 17/4/03) and from INTAS (grant no. 03-50-5765) is gratefully acknowledged. Support by J. Manz is gratefully acknowledged.

References

(1) Knowles, W. S. Asymmetric Hydrogenations (Nobel Lecture). *Angew. Chem. Int. Ed.* **2002**, *41*, 1999−2007.

(2) Noyori, R. Asymmetric Catalysis: Science and Opportunities (Nobel Lecture). *Angew. Chem. Int. Ed.* **2002**, *41*, 2008−2022.

(3) Sharpless, K. B. Searching for New Reactivity (Nobel Lecture). *Angew. Chem. Int. Ed.* **2002**, *41*, 2024−2032.

(4) Rice, S. A.; Zhao, M. *Optimal Control of Molecular Dynamics*; Wiley-VCH: Weinheim, 2001.

(5) Shapiro, M.; Brumer, P. *Principles of Quantum Control of Molecular Processes*; Wiley: Hoboken, NJ, 2003.

(6) Brixner, T.; Gerber, G. Quantum Control of Gas-Phase and Liquid-Phase Femtochemistry. *ChemPhysChem* **2003**, *4*, 418−438.

(7) Brumer, P.; Shapiro, M. Control of Unimolecular Reactions Using Coherent Light. *Chem. Phys. Lett.* **1986**, *126*, 541−546.

(8) Tannor, D. J.; Kosloff, R.; Rice, S. A. Coherent Pulse Sequence Induced Control of Selectivity of Reactions: Exact Quantum Mechanical Calculations. *J. Chem. Phys.* **1986**, *85*, 5805−5820.

(9) Green, D. S.; Bickel, G. A.; Wallace, S. C. (2+1) Resonance Enhanced Multiphoton Ionization of Hydrogen Chloride in a Pulsed Supersonic Jet: Spectroscopic Survey. *J. Mol. Spectrosc.* **1991**, *150*, 303−353.

(10) Green, D. S.; Bickel, G. A.; Wallace, S. C. (2+1) Resonance Enhanced Multiphoton Ionization of Hydrogen Chloride in a Pulsed Supersonic Jet: Spectroscopy and Rydberg ∼ Valence Interactions of the $^1\Sigma^+(0^+)$ and $^3\Sigma^-(1, 0^+)$ States. *J. Mol. Spectrosc.* **1991**, *150*, 354−387.

(11) Kvaran, A.; Wang, H. S.; Waage, B. G. Three- and Two-Photon Absorption Spectroscopy: REMPI of HCl and HBr. *Can. J. Phys.* **2001**, *79*, 197−210.

(12) Kvaran, A.; Wang, H. S. Three-Photon Absorption Spectroscopy: the $L(^1\Phi_3)$ and $m(^3\Pi_1)$ States of HCl and DCl. *Mol. Phys.* **2002**, *100*, 3513−3519.

(13) Yencha, A. J.; McConkey, A. G.; Dawber, G.; Avaldi, L.; MacDonald, M. A.; King, G. C.; Hall, R. I. Threshold Photoelectron Spectroscopy of HCl up to 40 EV. *J. Electron Spectrosc.* **1995**, *73*, 217−229.

(14) Yencha, A. J.; Cormack, A. J.; Donovan, R. J.; Hopkirk, A.; King, G. C. Threshold Photoelectron Spectroscopy of HCl and DCl. *Chem. Phys.* **1998**, *238*, 109−131.

(15) Edvardsson, D.; Baltzer, P.; Karlsson, L.; Lundqvist, M.; Wannberg, B. Rotational Fine Structure in the UV Photoelectron Spectra of HF and HCl. *J. Electron. Spectrosc.* **1995**, *73*, 105−124.

(16) Burmeister, F.; Andersson, L. M.; Ohrwall, G.; Richter, T.; Zimmermann, P.; Godehusen, K.; Martins, M.; Karlsson, H. O.; Sorensen, S. L.; Bjorneholm, O.; Feifel, R.; Wiesner, K.; Goscinski, O.; Karlsson, L.; Svensson, S.; Yencha, A. J. A Study of the Inner-Valence Ionization Region in HCl and DCl. *J. Phys. B: At., Mol. Opt. Phys.* **2004**, *37*, 1173−1183.

(17) de Beer, E.; Koenders, B. G.; Koopmans, M. P.; de Lange, C. A. Multiphoton Ionization Processes in Hydrogen Chloride Studied by Photoelectron Spectroscopy. *J. Chem. Soc., Faraday Trans.* **1990**, *86*, 2035−2041.

(18) de Beer, E.; Buma, W. J.; de Lange, C. A. Resonance Enhanced Multiphoton Ionization Photoelectron Spectroscopy and Pulsed Field Ionization Via the $F\ ^1\Delta_2(v' = 0)$ and $f\ ^3\Delta_2(v' = 0)$ Rydberg States of Hydrogen Chloride. *J. Chem. Phys.* **1993**, *99*, 3252−3261.

(19) Michel, M.; Korolkov, M. V.; Weitzel, K. M. State-Selective Predissociation Spectroscopy of HCl^+ and DCl^+ Ions. *J. Phys. Chem. A* **2004**, *108*, 9924−9930.

(20) Penno, M.; Holzwarth, A.; Weitzel, K. M. State Selective Predissociation Spectroscopy of Hydrogen Chloride Ions (HCl^+) Via the $A^2\Sigma^+ \leftarrow {}^2\Pi_{3/2}$ Transition. *Mol. Phys.* **1999**, *97*, 43−52.

(21) Saenger, K. L.; Zare, R. N.; Mathews, C. W. A Reexamination of the Spin-Rotation Constant for $^2\Pi$ States: The A−X Band System of HCl^+. *J. Mol. Spectrosc.* **1976**, *61*, 216−230.

(22) Korolkov, M. V.; Weitzel, K. M. The Predissociation Dynamics of Vibrational Eigenstates in the $A^2\Sigma^+$ State of HBr^+ Ions: Numerical Solution of Coupled Time-Dependent Schrödinger Equations. *Chem. Phys.* **2000**, *252*, 209−219.

(23) Korolkov, M. V.; Weitzel, K. M.; Peyerimhoff, S. D. Spin−Orbit Induced Predissociation Dynamics of HCl^+ and HBr^+ Ions: Temporal and Spectral Representations. *Int. J. Mass Spectrom.* **2000**, *201*, 109−120.

(24) Korolkov, M. V.; Weitzel, K. M. The Spin−Orbit Induced Predissociation Dynamics of HCl^+ Ions: Rotational Islands of Stability. *Chem. Phys. Lett.* **2001**, *336*, 303−310.

(25) Pradhan, A. D.; Kirby, K. P.; Dalgarno, A. Theoretical Study of HCl^+: Potential Curves, Radiative Lifetimes, and Photodissociation Cross Sections. *J. Chem. Phys.* **1991**, *95*, 9009−9023.

(26) Michel, M.; Korolkov, M. V.; Weitzel, K. M. A New Route to the Dissociation Energy of Ionic and Neutral HCl Via Lineshape Analysis of Single Rotational Transitions. *Phys. Chem. Chem. Phys.* **2002**, *4*, 4083−4086.

(27) Korolkov, M. V.; Weitzel, K. M. Kinetic and Dynamic Aspects of Lifetime Oscillations in the Predissociation of Hydrogen Chloride Ions. *J. Phys. Chem. A* **2006**, *110*, 2924−2932.

(28) Penno, M.; Holzwarth, A.; Weitzel, K. M. State Selective Predissociation Spectroscopy of Hydrogen Bromide Ions (HBr^+) Via the $^2\Sigma^+ \leftarrow {}^2\Pi_i(i=1/2, 3/2)$ Transition. *J. Phys. Chem. A* **1998**, *102*, 1927−1934.

(29) Kosloff, R. Propagation methods for quantum molecular dynamics. *Annu. Rev. Phys. Chem.* **1994**, *45*, 145.

(30) Feit, M. D.; Fleck, J. A.; Steiger, A. Solution of the Schroedinger equation by a spectral method. *J. Comput. Phys.* **1982**, *47*, 412.

(31) Korolkov, M. V.; Schmidt, B. Spin−Orbit Induced Association Under Ultrafast Laser Pulse Control. *Chem. Phys. Lett.* **2002**, *361*, 432−438.

(32) Korolkov, M. V.; Paramonov, G. K. Vibrationally State-Selective Electronic Excitation of Diatomic Molecules by Ultrashort Laser Pulses. *Phys. Rev. A: At., Mol., Opt. Phys.* **1998**, *57*, 4998−5001.

(33) Bisseling, R. N.; Kosloff, R.; Manz, J. Dynamics of hyperspherical and local mode resonance decay studied by time dependent wave packet propagation. *J. Chem. Phys.* **1985**, *83*, 993.

(34) Marquetand, P.; Engel, V. Predissociation and Dissociation Dynamics in Quantum Control Fields. *Chem. Phys. Lett.* **2005**, *407*, 471−476.

(35) Breunig, H. G.; Lauer, A.; Weitzel, K. M. Control of Branching Ratios in the Dissociative Ionization of Deuterium Chloride. *J. Phys. Chem. A* **2006**, *110*, 6395−6398.

CT600217T